Environmental Science Nano

ROYAL SOCIETY OF CHEMISTRY

PAPER

View Article Online
View Journal | View Issue

Check for updates

Cite this: *Environ. Sci.: Nano*, 2024, **11**, 1000

Submicron- and nanoplastic detection at low micro- to nanogram concentrations using gold nanostar-based surface-enhanced Raman scattering (SERS) substrates†

Jessica Caldwell, [a] Patricia Taladriz-Blanco, *[b] Laura Rodriguez-Lorenzo, [b] Barbara Rothen-Rutishauser [a] and Alke Petri-Fink *[ac]

Received 5th July 2023,
Accepted 29th November 2023

DOI: 10.1039/d3en00401e

rsc.li/es-nano

The presence of submicron- (1 μm–100 nm) and nanoplastic (<100 nm) particles within various sample matrices, ranging from marine environments to foods and beverages, has become a topic of increasing interest in recent years. Despite this interest, very few analytical techniques are known that allow for the detection of these small plastic particles in the low concentration ranges that they are anticipated to be present at. Research focused on optimizing surface-enhanced Raman scattering (SERS) to enhance signal obtained in Raman spectroscopy has been shown to have great potential for the detection of plastic particles below conventional resolution limits. In this study, we produce SERS substrates composed of gold nanostars and assess their potential for submicron- and nanoplastic detection. The results show 33 nm polystyrene could be detected down to 1.25 μg mL^{-1} while 36 nm poly(ethylene terephthalate) was detected down to 5 μg mL^{-1}. These results confirm the promising potential of the gold nanostar-based SERS substrates for nanoplastic detection. Furthermore, combined with findings for 121 nm polypropylene and 126 nm polyethylene particles, they highlight potential differences in analytical performance that depend on the properties of the plastics being studied.

Environmental significance

Submicron- and nanoplastics are anticipated to be as ubiquitous within our surrounding environment as microplastics. However, to date, relatively few analytical techniques exist which allow for their detection at low (environmentally relevant) concentrations. Surface-enhanced Raman scattering spectroscopy has been highlighted as a promising means to fill this analytical gap and allow for more in-depth analysis of samples containing submicron- and nanoplastics. Yet, many common plastic types reported to be found in environmental and food samples have not been comprehensively studied with this technique. Herein, the authors utilize gold nanostars to try to facilitate detection of a variety of common plastic types (*i.e.*, polystyrene, poly(ethylene terephthalate), polypropylene, and polyethylene) at concentrations as low as 625 ng mL^{-1} in some cases.

Introduction

Within the past decade, there has been a growing interest in developing analytics that allow for the study of small plastic particles, namely submicron- (1 μm–100 nm) and nanoplastics (<100 nm),[1] within complex matrices such as foods and beverages,[2] environmental water,[3,4] polar ice,[5] or wastewater.[6] Such studies have reported particle concentrations on the order of ng mL^{-1} (*e.g.*, 13.2 ng mL^{-1} in ice cores from Greenland,[5] 52.3 ng mL^{-1} in ice cores from Antarctica,[5] 4.2 ng mL^{-1} in Wadden Sea water,[3] and 13–16 μg in a single cup of tea[2]). However, very few studies have managed to detect nanoplastics within complex environmental or food samples.[7,8] Furthermore, concern has been raised regarding the reliability of data currently being

[a] *Adolphe Merkle Institute, University of Fribourg, Chemin des Verdiers 4, 1700 Fribourg, Switzerland. E-mail: alke.fink@unifr.ch*
[b] *Water Quality Group, International Iberian Nanotechnology Laboratory (INL), Av. Mestre Jose Veiga s/n, 4715-330, Braga, Portugal. E-mail: patricia.taladrizblanco@unifr.ch*
[c] *Department of Chemistry, University of Fribourg, Chemin du Musée 9, 1700 Fribourg, Switzerland*

† Electronic supplementary information (ESI) available: A word file containing 8 figures and 2 tables in 12 pages. These figures and tables contain additional information for the physicochemical characterization of all particle types, characterization data for 43 nm AuSphere-based substrates, all Raman and SERS control data, measurement parameters for all Raman and SERS measurements, and detailed peak assignments for each plastic type studied. See DOI: **https://doi.org/10.1039/d3en00401e**

reported,[7] and the current state-of-the-art relies heavily on destructive thermal techniques[3–6] that prevent measurement repetition for a given sample.

One proposed method for improving submicron- and nanoplastic detection is the use of a modified version of Raman spectroscopy. Raman spectroscopy is a vibrational spectroscopy technique that gives material-specific information about the sample of interest through monitoring the inelastic scattering of an initial excitation laser that has interacted with the sample (*i.e.*, Raman scattering).[9] It is heavily utilized in studies of larger microplastic (5 mm–1 μm)[1] particles as it allows for their detection and differentiation without staining or labeling and is non-destructive.[10] However, its application to smaller plastic particles requires adaptation of the standard method as it has a size limit of ~1 μm[10] that is influenced by the conventional resolution limitations of optical measurements and the low probability for a sample to Raman scatter.[9,11,12] Some strategies have been employed in the field to date to circumvent this conventional limitation. One such example is the optical trapping of dispersed particles for Raman measurements in a technique called Raman tweezers (or optical tweezers).[13] However, this trapping must be carefully tailored to the size and refractive index of the particle of interest, and at small sizes there is an increased risk that Brownian diffusion of the particles will break the required trapping and prevent sample measurement.[13] To avoid this limitation, Raman signal can instead be enhanced through the introduction of a corrugated plasmonic metal, commonly silver (Ag) or gold (Au), in an approach known as surface-enhanced Raman spectroscopy (SERS).[14] Through SERS, researchers take advantage of collective oscillations of electrons at the metal surface to enhance the intensity of Raman scattering signals obtained from samples placed within a 10 nm range; a process which can be observed for samples in dispersed or dry states without the need for optical trapping.[14] SERS substrates are heavily used for the analysis of samples containing small molecules (*e.g.*, samples of pharmaceuticals, chemical compounds from explosives in water), with a multitude of protocols established for creation of different substrate types.[11,14] These studies have indicated an optimized SERS substrate can allow for single molecule detection, and can improve the Raman signal obtained by factors up to $\sim 10^{14}$.[14]

Within recent years, the use of SERS has gained some traction within the field of submicron- and nanoplastics research, and multiple studies have been released to highlight the potential of SERS for their detection. These studies have employed a variety of plasmonic systems to generate SERS signal, including, among others, aggregation of spherical Ag nanoparticles (AgSpheres)[15,16] or spherical Au nanoparticles (AuSpheres)[17] around plastic samples, assembly of Ag nanowires[18,19] or Au nanocrystals[20] through filtration, soaking filter paper with AuSpheres,[21] trapping Ag-coated Au nanostars in pre-designed templates,[22] and assembly of AuSpheres onto functionalized glass.[23] These strategies can be loosely sorted into two categories: studies that aim to generate regions of strong SERS enhancement (*i.e.*, hotspots) through the aggregation of spherical nanoparticles that have low enhancing capabilities in the single-particle state, and creation of SERS substrates using anisotropic particles which have higher enhancing capabilities at the single-particle state (*e.g.*, nanowires, nanocrystals, and nanostars) due to intrinsic hotspots that form along sharp edges present in the particles.[14] Literature focused on SERS detection of small molecules has highlighted the latter category as capable of generating the highest SERS enhancements at lower particle concentrations.[14] While only a small body of literature exists for SERS substrates used for plastics detection, it can already be observed that this trend is carried over into submicron- and nanoplastics research. In previous studies, the authors demonstrated the detection of 161 nm polystyrene (PS) down to 10 μg mL^{-1} and 33 nm PS down to 20 μg mL^{-1} on AuSphere-based SERS substrates.[23] In contrast, Qin *et al.* demonstrated the detection of 100 nm PS down to 100 ng mL^{-1} and of 20 nm PS on Au nanocrystals trapped in glass fiber filters.[20]

Despite these promising initial findings, much remains unknown about the potential of SERS with anisotropic plasmonic particles for submicron- and nanoplastic detection. The vast majority of studies published to date have focused their efforts on a limited number of plastic types, most commonly PS alone,[16,18,20–22] and many have yet to look at the detection of particles below 50 nm in size.[15–19,22] To begin addressing these knowledge gaps, this study focuses on the detection of 5 different types of submicron- and nanoplastics (*i.e.*, 161 nm PS, 33 nm PS, 36 nm poly(ethylene terephthalate) (PET), 121 nm polypropylene (PP), and 126 nm polyethylene (PE)) with SERS substrates using anisotropic gold nanostars (AuStars) assembled on functionalized glass.

Materials and methods

Materials

Tetrachloroauric acid ($HAuCl_4 \cdot 3H_2O$, 99.9%), sodium citrate tribasic dihydrate ($C_6H_5Na_3O_7 \cdot 2H_2O$, 99.5%), sodium dodecyl sulfate (SDS; ACS reagent; $NaC_{12}H_{25}SO_4$; 99.9%), (3-aminopropyl) triethoxysilane (APTES; $C_9H_{23}NO_3Si$; 99%), poly(allylamine hydrochloride) (PAH; $[CH_2CH(CH_2NH_2 \cdot HCl)]_n$; average Mw 17 500), *N*,*N*-dimethylformamide (DMF; $HCON(CH_3)_2$; anhydrous, 99.8%), *m*-xylene (C_8H_{10}; >99%), PP (isotactic; $[C_3H_6]_n$) pellets, and styrene (ReagentPlus® reagent; C_8H_8; 99.9%) were purchased from Sigma-Aldrich, Switzerland. Toluene ($C_6H_5CH_3$; AR certified for analysis) was purchased from Fisher Scientific, Switzerland. Absolute ethanol (C_2H_6O; 99.9%) was purchased from VWR chemicals, Switzerland. PE (low density; $[C_2H_4]_n$) pellets were purchased from Sigma Aldrich, USA. Sodium chloride salt (NaCl; >99.5%) was purchased from Carl Roth GmbH + Co. KG, Germany. PET ($[C_{10}H_8O_4]_n$) pellets were purchased from Goodfellow Cambridge Ltd., UK. Hydroxylamine hydrochloride ($NH_2OH \cdot HCl$, 99.0%) and potassium peroxodisulfate (KPS; ACS reagent; $K_2S_2O_8$, 99.9%) were purchased from Fluka, Switzerland.

Polyvinylpyrrolidone (PVP; $[C_6H_9NO]_n$; Mw 10 000) and hexafluoroisopropanol (HFIP; $C_3H_2F_6O$; >99%) were purchased from Tokyo Chemical Industry Co., Ltd. (TCI) in Japan. Hydrogen peroxide (H_2O_2, 30 wt% in H_2O) was purchased from Reactolab SA, Switzerland. Sulfuric acid (ISO + Ph. Eur. Reagent; H_2SO_4, 95%) was obtained from Honeywell, Germany. All water referred to as Milli-Q within the manuscript was purified with an 18.2 MW cm arium 611DI Milli-Q system (Sartorius Stedim Biotech, Germany) prior to use.

Preparation of Au nanoparticles (AuNPs) and plastic particles

The synthesis of 43 nm AuSpheres was conducted as previously described.[23] Briefly, Au seed particles were synthesized with a modified Turkevich method[24] and then utilized for seeded growth synthesis through a modified version of the Brown method.[25]

Synthesis of 79 nm AuStars was conducted following a modified version of the protocol reported by Senthil Kumar *et al.*[26] 10 mL of Au seeds were functionalized with PVP through the dropwise addition of 1 mL of a 0.0163 g mL^{-1} PVP solution while shaking. The solution was left to react overnight on the shaker plate prior to up-concentration and cleaning *via* centrifugation. Seeds were re-dispersed in absolute ethanol, and their concentration was checked with ultraviolet-visible (UV-vis) spectroscopy. Next, 10 g of PVP was dissolved in 100 mL of DMF at room temperature by stirring. A salt solution of $HAuCl_4$ was introduced to obtain a final Au concentration of 0.5 mM and was left stirring for 3 min. Then, PVP functionalized seed particles were introduced such that their final concentration in the reaction mixture was 0.023 mM (of Au^0). The reaction was left to stir for 30 min, then checked with UV-vis spectroscopy to ensure the particles had obtained a star-like morphology. AuStars were then centrifuged once to clean and re-dispersed at a concentration of 0.5 mM Au^0 in absolute ethanol. Prior to SERS substrate creation, AuStar dispersions were centrifuged twice more, with the first redispersion in absolute ethanol and the final in Milli-Q water.

The syntheses of 161 nm and 33 nm PS was reported previously.[23] Briefly, both particle stocks were created through an emulsion polymerization approach utilizing a KPS initiator for styrene polymerization and SDS to form the emulsion under inert atmosphere. Particle sizes were controlled using varied temperature, reaction time, and surfactant ratios.

The preparation of 36 nm PET, 126 nm PE, and 121 nm PP particles was conducted following a reprecipitation protocol first reported by Muff *et al.*[27] An appropriate solvent was selected for the dissolution of the bulk polymer, which varied depending on the type of polymer being worked with. Further adaptations to reaction conditions (*e.g.*, temperature, presence of surfactant in the antisolvent) were also adapted to suit the polymer used for the reprecipitation. For 36 nm PET, HFIP was used to dissolve 5 mg mL^{-1} polymer pellets at room temperature by placing the mixture in a vial on a shake plate for 24 h. The antisolvent for PET reprecipitation was Milli-Q water. For 126 nm PE, toluene was used to dissolve 5 mg mL^{-1} polymer pellets with the use of mild heat from a heat gun, while for 121 nm PP, *m*-xylene was used to dissolve 5 mg mL^{-1} polymer pellets with the help of a reflux column and an oil bath at 140 °C. The antisolvent for both PE and PP was Milli-Q water with 2.5 mg mL^{-1} of NaCl and 5 mg mL^{-1} of SDS. All reprecipitations were conducted by injecting the polymer solutions and antisolvents simultaneously into a confined impinging jet (CIJ) Teflon mixer and collected in a beaker of antisolvent below.[27] All final plastic particle dispersions in Milli-Q water were then filtered with a 1 μm cutoff polytetrafluoroethylene (PTFE) syringe filter (Sigma Aldrich, Switzerland) and dialyzed against Milli-Q water for 7 d with a 14 kDa cellulose membrane (Carl Roth GmbH + Co, Switzerland).

All particle types were stored in glass containers at 4 °C when not in use.

Characterization of AuNPs and plastic particles

Initial characterization of all AuNP dispersions was conducted using UV-vis extinction spectra. All spectra were recorded for particle dispersions in quartz Suprasil cuvettes (Hellma Analytics, Germany) with a V-670 spectrophotometer (Jasco, USA) at room temperature using a 10 mm path length.

Hydrodynamic diameters and zeta potentials of all AuNP and plastic particle dispersions were measured in disposable cuvettes (Kartell S.p.A., Italy) using a 90Plus Particle Size Analyzer (Brookhaven Instruments Corporation, USA; measurement angle 90°; 40 mW diode laser; λ = 640 nm) with phase-amplitude light scattering (PALS) for zeta-potential determination (Brookhaven Instruments, USA). The analysis was carried out in diluted suspensions in Milli-Q water at room temperature.

To obtain primary size data for AuNPs, a Tecnai Spirit transmission electron microscope (TEM; FEI, USA) operating at 120 kV was used. 10 μL of particle dispersion was cast onto TEM grids (carbon film on copper 300 square mesh; Electron Microscopy Sciences, USA) and dried at room temperature before imaging the particles with a Veleta wide-angle CCD camera (2048 × 2048 pixel; Olympus, Japan). TEM images were processed with the ImageJ software (v1.53). Average AuNP size and standard deviation were measured manually in Fiji (ImageJ; Wayne Rasband National Institute of Health, USA) by drawing lines through the largest diameter for each spherical particle or from the end of one star tip to the end of another tip in the longest continuous line through the particle that was possible.

PS, PET, PE, and PP particles were imaged using a scanning electron microscope (SEM, TESCAN Mira 3 LM field emission, Kohoutovice, Czech Republic). Briefly, 10 μL of stock particles (diluted for PET and PS but unaltered for PE and PP) were dried at room temperature on glass coverslips affixed to aluminum SEM stubs (Agar Scientific, UK) with carbon black tape (Agar Scientific, UK). Dried samples were sputter coated with a 2 nm thick layer of gold using a 208 HR

sputter coater (Cressington Scientific Instruments, UK). Average particle size and standard deviation were measured manually in Fiji by drawing lines through the largest possible diameter for each particle.

Mass concentration of the 36 nm PET nanoplastic was determined through mass balancing particle powders (dried at 70 °C overnight) obtained from a fixed (500 μL) volume using an AG204 Delta Range balance (Mettler-Toledo GmbH, Switzerland). This process was repeated three times to obtain the final average stock concentration. 126 nm PE and 121 nm PP mass concentrations were obtained through nanoparticle tracking (NTA) analysis (PANalytical NanoSight NS300; Malvern Instruments, UK). The particles were excited with a 488 nm CW laser, injected at an infusion speed of 100 into the glass flow-cell top-plate, and sealed with a polydimethylsiloxane (PDMS) ring. For 126 nm PE, a measurement camera gain of 2 and level of 9 were used with 5, 60 s captures, then the data was processed with a screen gain of 7 and a threshold of 10 to obtain the final concentration values. For 121 nm PP, a measurement camera gain of 2 and level of 8 were used with 5, 60 s captures, then the data was processed with a screen gain of 8 and a threshold of 10 to obtain the final concentration values. The flow-cell top plate was thoroughly cleaned between samples using Milli-Q water.

SERS substrate fabrication and characterization

The creation of SERS substrates using 43 nm AuSpheres was conducted using the same layer-by-layer (LbL) protocol previously reported.[23] This protocol was then adapted to accommodate the preparation of SERS substrates through LbL assembly with AuStars. First, glass slides were cut into 10 mm × 25 mm pieces that were piranha washed (1 : 3 ratio by volume of H_2O_2 : H_2SO_4) for 30 min. Clean glass was Milli-Q rinsed and dried with N_2 before soaking for 4 h in an APTES solution (2 vol% APTES in absolute ethanol). APTES functionalized glass was rinsed with absolute ethanol to condense the APTES on the surface, then Milli-Q water to remove excess, and N_2 dried. APTES functionalized glass was then soaked for 24 h in a 0.5 mM [Au^0] dispersion of AuStars in Milli-Q, rinsed with Milli-Q and dried overnight in air.

All SERS substrate batches were characterized first with UV-vis spectroscopy and then SEM. For SEM, a substrate was affixed to an aluminum SEM stub using carbon black tape and silver paste around the edges. Substrate samples were sputter coated with 2 nm of gold and imaged.

Raman and SERS spectroscopy

Each plastic sample measured was drop-cast in 5 μL volumes onto the surface of the respective substrate and dried at room temperature prior to measurement. Raman and SERS measurements were conducted with a WiTec Alpha 300 R confocal Raman microscope or a WITec Alpha300 Access confocal Raman microscope. Both microscopes were operated with a 785 nm laser wavelength, 50× objective, and a built-in CCD camera for bright field imaging (WITec, Germany). Individual spectra were collected by accumulating multiple (*i.e.*, 150–750) scans of 0.5–1 s to generate a final average spectrum. Laser power ranged from 1 mW to 10 mW depending on the sample and substrate used. Exact measurement details for every sample are given in Table S1.† SERS spectra presented for plastic particle samples were reproducible, and collected from various positions within the final, dried sample.

All confocal Raman spectra were corrected (*i.e.*, cosmic ray filters were applied, the measured background spectrum of each slide was subtracted from the sample data collected, and a polynomial baseline subtraction filter was applied) using the accompanying WITec Control 5 software.

Contamination prevention

Cotton lab coats and latex gloves were worn when samples were being handled. Particle syntheses were conducted in laminar flow hoods, and LbL assembly of SERS substrates was conducted in sealed containers. Glass containers were used during particle synthesis, to hold particle dispersions, and during SERS substrate preparation. When the samples were not actively being worked with, they were left in sealed containers. Blank controls were measured for all analytical techniques utilized for plastic particles to ensure any potential atmospheric deposition of contaminants or signals from sample supporting materials were accounted for.

Results and discussion

Creation of particle stocks and SERS substrates

Physicochemical characterization results from DLS, zeta potential, and electron microscopy measurements are summarized in Table 1. SEM imaging indicated that all plastic particles, regardless of the type of plastic and synthesis utilized, had core sizes below 200 nm and were predominantly spherical in shape (Fig. S1†). Blank controls prepared for SEM images indicated that there was no particulate matter contamination as a result of sample preparation that would interfere with accurate sizing of the plastic particles (Fig. S2†). Throughout this manuscript, the submicron- and nano-sized particles of PS will be referred to as 161 nm and 33 nm PS, respectively, to facilitate comparison of the data presented in previous work using these particle stocks.[23]

As a result of their hydrophobicity,[1] reprecipitation of PE and PP has a low particle yield compared to PET. The stock concentration measured by NTA for 126 nm PE was 2.4 μg mL^{-1}, and for 121 nm PP was 1.7 μg mL^{-1}. These samples were used without further dilution for all sample characterization and SERS measurements. The stock concentration measured for 36 nm PET through mass balancing was 755 μg mL^{-1}, so serial dilutions of the particles could be prepared for subsequent analysis.

In addition to the differences in yield of the plastic particles, it can also be noted that there is a higher standard deviation in core sizing measurements for 121 nm PP and 126 nm PE than for the comparably sized 161 nm PS. This indicates a slightly higher heterogeneity of the PE and PP

Table 1 A summary of key physicochemical properties for all presented submicron- and nanoparticles

	Core Size[a] (nm)	Hydrodynamic diameter (nm)	Zeta potential (mV)
161 nm PS	147 ± 17	179 ± 6	−37 ± 2
33 nm PS	34 ± 7	50 ± 12	−39 ± 5
36 nm PET	36 ± 9	55 ± 1	−25 ± 9
121 nm PP	121 ± 47	207 ± 3	−25 ± 5
126 nm PE	126 ± 48	216 ± 5	−23 ± 7
79 nm AuStars	79 ± 9	99 ± 1	−14 ± 4
43 nm AuSpheres	43 ± 5	50 ± 1	−26 ± 8

[a] AuNP sizing was conducted using TEM images while plastic particle sizing was performed using SEM images. For all samples, a minimum of 200 particles were sized.

particles compared to the other plastic particle types and is reflected in the higher difference between the average core size measured with SEM and the hydrodynamic size measure with DLS. Calculating light scattering results is strongly dependent on particle radius, which leads to the portion of the particle population with larger radii dominating measurements and skewing the final hydrodynamic size reported.[28]

Seeded growth in the presence of citrate following the adapted Brown method[25] yielded citrate-stabilized AuSpheres with an average size of 43 nm. The introduction of PVP to the seed surface prior to following the adapted protocol of Kumar *et al.*[26] allowed for the synthesis of AuStars having an average of 79 nm in size (Table 1). The hydrodynamic diameter of 99 nm for the AuStars was calculated by approximating a sphere of comparable size diffusing at the same speed observed for the anisotropic particles *via* the Stokes–Einstein equation.[28] Both types of gold particles had negative surface charges. Thus, the SERS substrate creation required a LbL assembly protocol which introduced a positive charge to the glass surface through functionalization. SERS substrates fabricated with 43 nm AuSpheres utilized a piranha wash step followed by PAH functionalization to achieve this (Fig. S3†), as previously reported.[23] However, for 79 nm AuStars, the protocol was adapted so that the piranha-washed glass surface was functionalized with APTES (see Materials and methods section for more details). The smaller size of APTES compared to PAH allowed AuStars to be assembled on the surface with more distance between particles (Fig. 1). This approach prevented an overlap of surface plasmons from multiple AuStars, which is important as the excitation laser wavelength must be matched to the plasmonic behavior of the SERS substrate for optimum measurement conditions.[14] Unlike AuSpheres, where the overlap of plasmons from multiple particles is used to create SERS hotspots without shifting the excitation wavelength required outside of the visible–near infrared range,[14,23] a high amount of overlap of AuStars plasmons could shift the excitation wavelength required for SERS outside of the range available on the Raman instruments being utilized and hinder subsequent sample analysis.[14]

While it is likely that some slight overlap of 79 nm AuStar plasmons may be occurring, as indicated by the formation of a "tail" of slightly stronger absorbance in the UV-vis spectrum of the SERS substrates near the 1100–1200 nm region when compared to the particles in their dispersed state, the strongest signal can still be observed within the visible–near infrared wavelength range (Fig. 1). This observation is further supported

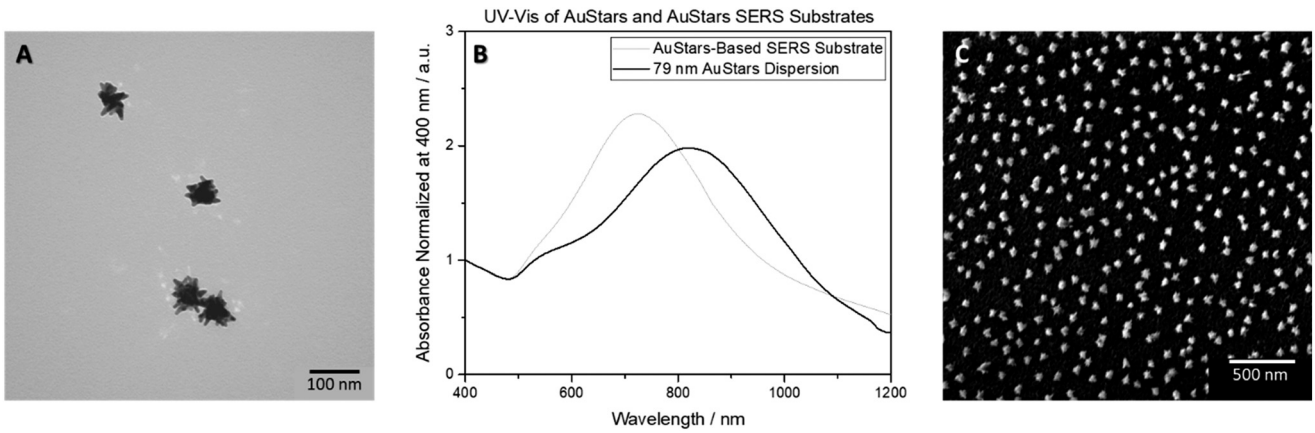

Fig. 1 An overview of the properties of the AuStars both in dispersion and assembled to create SERS substrates. A) A TEM image of AuStars. B) A UV-vis spectrum of the AuStars in Milli-Q water compared with a UV-vis spectrum of a SERS substrate. C) A representative SEM image of an AuStar-based SERS substrate.

by SEM imaging of the SERS substrates that show a random distribution of predominantly single AuStars around the surface. This protocol could be utilized to create SERS substrates using AuStars from different syntheses. The substrates were considered viable for measurements with submicron- and nanoplastic samples drop-cast onto their surface.

Submicron- and nanoplastic detection with AuStar-based SERS substrates

Reference measurements of PS, PET, PP, and PE microparticles (Fig. S4†), and high-concentration stocks of 161 and 33 nm PS, and 36 nm PET particles (Fig. S5†) were

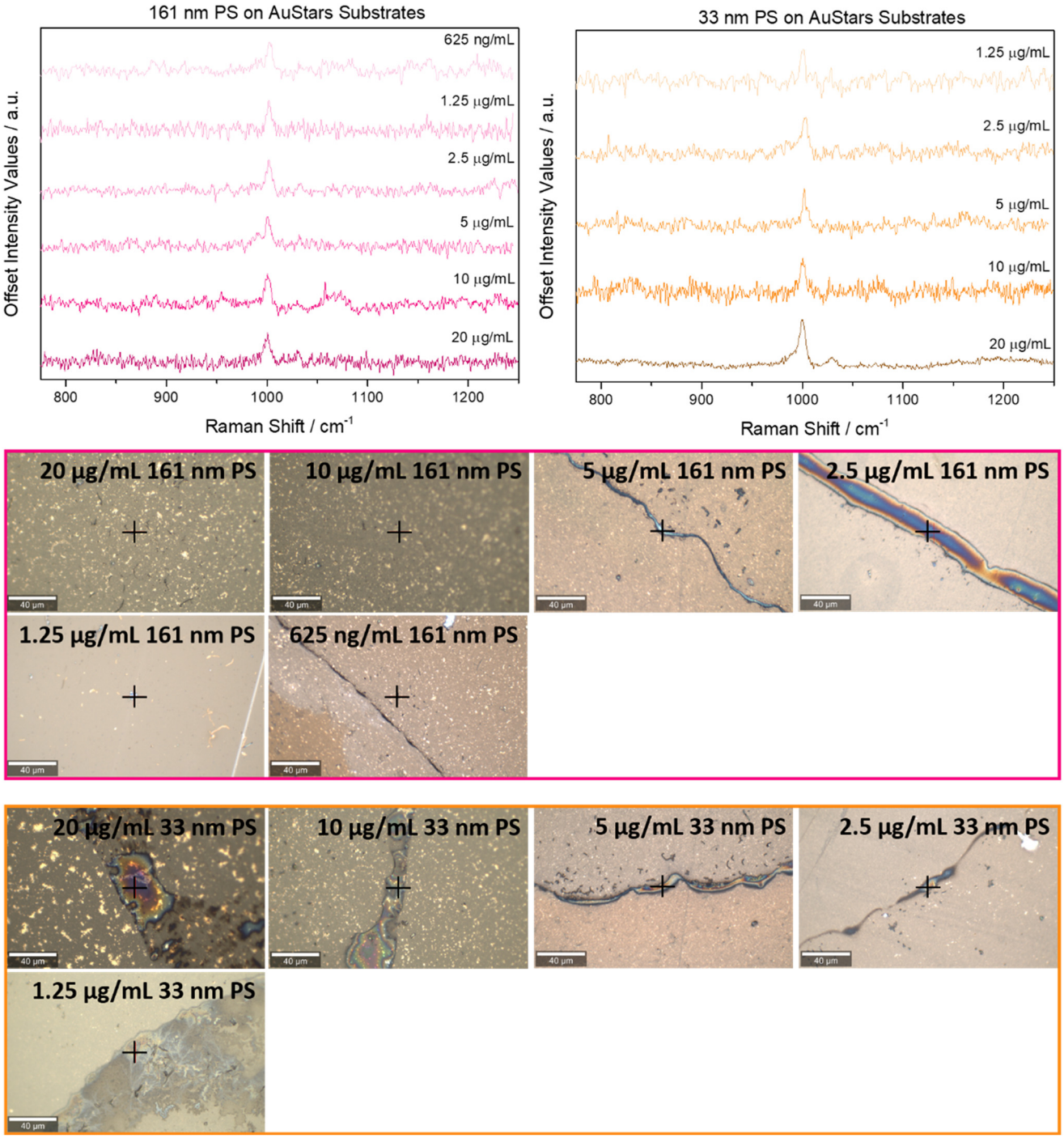

Fig. 2 Upper left: representative SERS spectra for all concentrations it was possible to detect the 161 nm PS submicronplastics at. Upper right: representative SERS spectra for all concentrations it was possible to detect the 33 nm PS nanoplastics at. Bottom: brightfield images of the regions of interest from which the SERS spectra were obtained. Exact measurement positions are indicated with black crosses. Scale bar is 40 μm for all samples. Full measurement parameters for each sample can be viewed in Table S1.†

used to identify the spectral region of interest for the SERS measurements. For PS, two peaks at 1002 cm^{-1} and 1032 cm^{-1}, indicative of ring breathing and CH in-plane deformation in PS,[29] are monitored. 36 nm PET was detected using two peaks present at ~1617 and 1730 cm^{-1} as a result of aromatic bending and carbonyl stretching,[30,31] while attempts to identify PP and PE were made using peaks present from 2840–2952 cm^{-1} as a result of various CH_2 and CH_3 stretching vibrations.[31,32] All spectral regions identified for each plastic type agreed with previously reported literature values.[10,23] Full descriptions of peak positions with their corresponding vibrational modes and assignments can be found in Table S2.†

The limit of detection (LOD) previously reported for 33 nm PS particles on AuSpheres-based SERS substrates was 20 μg mL^{-1},[23] thus, this was the concentration selected to be the starting point for SERS measurements with AuStars-based substrates. Both 161 nm and 33 nm PS particles could be successfully detected at this concentration during the SERS measurements (Fig. 2). Serial dilutions of both PS particle types were then prepared and analyzed to determine their LODs on AuStars-based substrates. The 161 nm PS submicron plastics generated a signal at 1002 cm^{-1} that could be monitored down to a concentration of 625 ng mL^{-1} (Fig. 2, upper left panel). 33 nm PS nanoplastic presence could be assessed down to a concentration of 1.25 μg mL^{-1} (Fig. 2, upper right panel). It is likely that this difference in the detection limit between the two types of PS particles is directly related to the particle properties. In this instance, the size of the particles being analyzed in the SERS measurements will likely influence the SERS substrates' analytical potential.

As further proof that the signals obtained were indeed the result of SERS signal enhancements, each concentration it was possible to detect the PS particles at using the AuStars-based substrates was drop-cast onto a clean glass slide and measured with regular Raman (Fig. S6†). For all Raman controls of this nature, no signal was observed at 1002 and 1032 cm^{-1}, confirming that AuStars substrates were required for the sample detection.

36 nm PET nanoplastics were also analyzed using a starting concentration of 20 μg mL^{-1}. On the AuStars-based substrates, it was possible to detect the 1617 cm^{-1} peak for 36 nm PET at

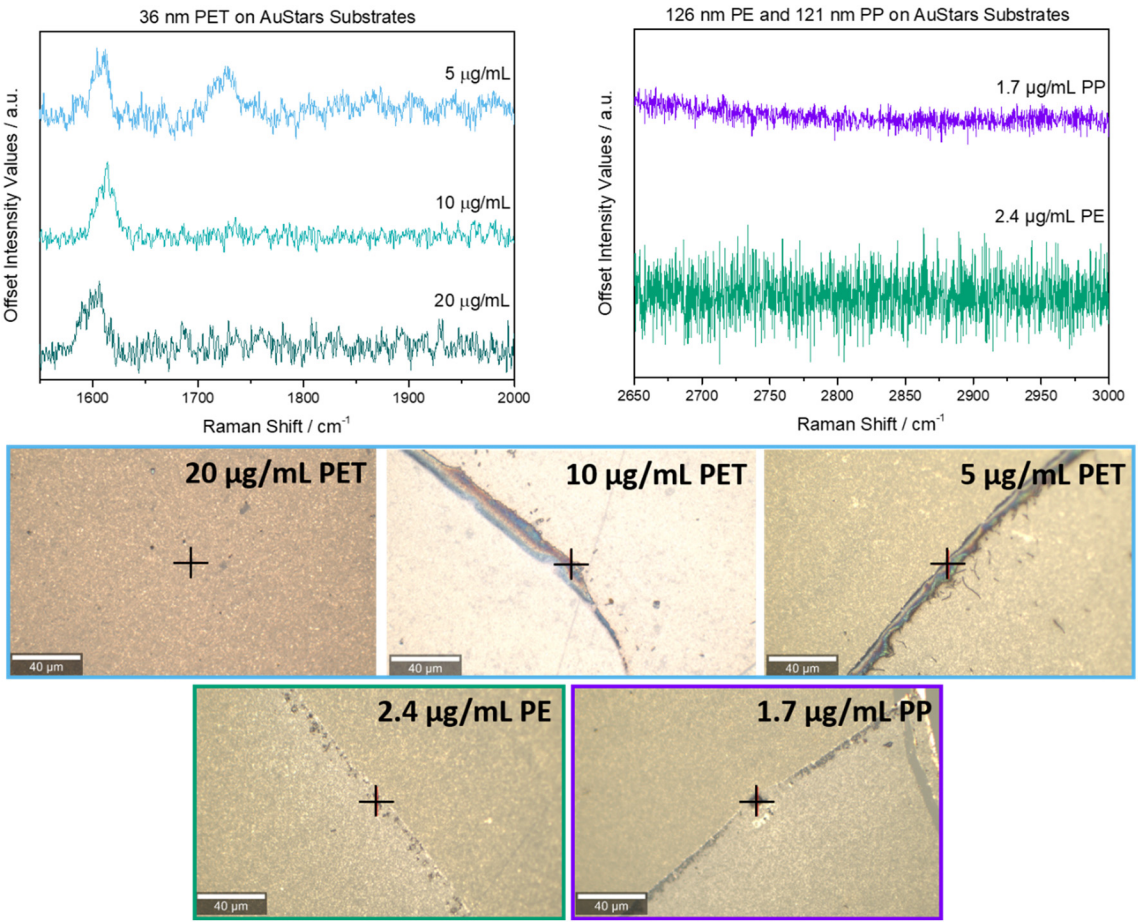

Fig. 3 Upper left: representative SERS spectra for all concentrations it was possible to detect the 36 nm PET nanoplastics at. Upper right: representative SERS spectra for measurement attempts made at the stock concentrations of 126 nm PE and 121 nm PP submicronplastics. Bottom: brightfield images of the regions of interest that the SERS spectra were obtained from. Exact measurement positions are indicated with black crosses. Scale bar is 40 μm for all samples. Full measurement parameters for each sample can be viewed in Table S1.†

concentrations as low as 5 μg mL^{-1} (Fig. 3, upper left panel). Attempts to measure the 20 μg mL^{-1} sample of 36 nm PET on the AuSpheres-based substrates were unsuccessful (Fig. S7†), and the control samples measured with regular Raman also did not show any signal at 1617 cm^{-1} or 1730 cm^{-1} (Fig. S8†). Thus, it is clear that the use of AuStars-based substrates was required to facilitate the 36 nm PET detection.

Interestingly, despite being within a comparable size range to the 33 nm PS nanoplastics, the LOD for 36 nm PET nanoplastics was higher (*i.e.*, 5 μg mL^{-1} for 36 nm PET compared to 1.25 μg mL^{-1} for 33 nm PS). This finding indicates that there is likely an influence on SERS detection that comes not just from the plastic particle size but also the type of plastic being studied. Taking in account the Raman selection rules, the vibration of a specific functional group will be Raman-active if the polarizability is changed during this vibration.[33] For this reason, the vibration modes assigned to the benzene group in both PET and PS present high Raman cross-sections. However, the difference in the LOD may be attributed to the orientation of the benzene in respect to the gold surface. PET involves a carboxylic acid-substituted benzene, and this structural difference may have an effect on the chain conformation; provoking the benzene groups to adopt a perpendicular orientation on the surface and influencing enhancement of the SERS signal of the PET particles.[34]

Next, to further probe the influence of plastic type on LODs of AuStars substrates, measurements were attempted for plastic particle types that did not contain aromatic bonds (Table S2†). With sizes of 121 nm for PP and 126 nm for PE falling between the 161 nm and 33 nm sizes of the PS particles, one would anticipate their LOD should be within the same concentration range if plastic particle size were the only factor influencing SERS results. However, at the stock concentrations, no signal was observed in the 2840–2952 cm^{-1} region during SERS measurements with AuStars and AuSpheres-based substrates (Fig. 3 and S7†).

While the concentrations of 126 nm PE and 121 nm PP are low, they still fall above the LOD of 625 ng mL^{-1} reported for 161 nm PS as well as the 1.25 μg mL^{-1} LOD reported for 33 nm PS nanoplastics. This finding is likely because aromatic carbon bonds are more polarizable and thus will yield a stronger Raman signal than aliphatic carbon bonds as commented above.[35–37] With this in mind, it becomes clear that the properties of the studied plastic particles have the potential to influence the applicability of analytical methods such as SERS. Thus, researchers hoping to validate a new analytical technique for plastics should be strongly encouraged to work with a wide variety of plastic particle types (*e.g.*, vary the plastic type, size, shape, presence of additives, and other physicochemical properties as possible) to gain an in-depth understanding of the factors influencing analysis.

Control spectra were collected from SERS substrates and glass slides without plastic particles as a final check. The signal observed in these measurements is attributed predominantly to the autofluorescence signal of the glass and does not show sharp peaks in the studied spectral regions for any of the plastics (Fig. S8†). This confirms there was no signal coming from the SERS substrates (*e.g.*, from the functionalization, residual materials from the synthesis of the AuStars or AuSpheres, dust, or other contaminants at high concentrations) that would interfere with submicron- and nanoplastic analysis.

Comparison of SERS substrates for plastic particle detection

The 161 nm PS and 33 nm PS particles could be detected on AuStars-based SERS substrates at a concentration an order of magnitude lower than previously reported values for AuSpheres substrates (Table 2). 36 nm PET particles could be detected at concentrations that were a quarter of the AuSpheres-based LOD. Furthermore, the LOD for the 36 nm PET on AuStars is also a third of the 15 μg mL^{-1} LOD previously reported for larger 62 nm PET nanoparticles on AuSpheres substrates.[23] Such a comparison highlights the impact of using anisotropic gold particles (AuStars) in the place of isotropic (AuSpheres) for creating the SERS substrates and aligns well with literature summarizing studies that focused on the detection of small molecules.[14] In addition to mass-based concentrations, Table 2 also contains an estimated number of particles per sample drop applied to the SERS substrates. It is important to note that these values are tabulated using an average core size (reported in Table 1) and density (*i.e.*, 1.08 g cm^{-3} for PS, 1.39 g cm^{-3} for PET, 0.9 g cm^{-3} for PP, and 0.93 g cm^{-3} for PE). Thus, these values are

Table 2 A summary of the LODs for all presented submicron- and nanoplastics on SERS substrates composed of AuSpheres and AuStars. In addition to mass based LODs, the lowest concentration measured is reported as an estimated total number of particles within the final sample drop applied to the substrate. PE and PP particle number values are reported for the drop applied at stock concentration for comparison

Plastic sample	SERS LOD on AuSpheres (μg mL^{-1})	Approximate plastic particle number on AuSpheres	SERS LOD on AuStars (μg mL^{-1})	Approximate plastic particle number on AuStars
161 nm PS	10[a]	9.84×10^9	0.625	3.08×10^8
33 nm PS	20[a]	4.24×10^7	1.25	1.32×10^6
36 nm PET	20	5.89×10^9	5	7.36×10^8
121 nm PP	Not detectable	2.46×10^7	Not detectable	1.23×10^7
126 nm PE	Not detectable	2.04×10^7	Not detectable	1.02×10^7

[a] Data adapted from Caldwell *et al.*, Nanomaterials, 2021.[23]

subject to some variability which increases with increasing polydispersity of the plastic particle dispersions.

As the vast majority of studies focused on the optimization of SERS for the detection of submicron- and nanoplastic particles have worked with PS, it is the easiest plastic type to use for comparison of system performance. Kihara *et al.* report the reliable detection of 20 and 200 nm PS particles on substrates composed of 20 nm AuSpheres on filter paper at concentrations down to 5–10 μg mL^{-1}.[21] These values are comparable with the work previously conducted using AuSpheres-based SERS substrates assembled onto glass.[23] Still, they are up to an order of magnitude higher than those reported for AuStars-based substrates in this study. Yang *et al.* reported the fabrication of SERS substrates created by capturing Ag nanowires on a filter and detecting PS particles with sizes ranging from 1 μm to 50 nm that, when paired with a higher-energy 633 nm laser, were demonstrated to detect PS on the order of 10^{-7} g L^{-1} (100 ng L^{-1} or 100 pg mL^{-1}).[19] Furthermore, they reported a trend of observing stronger signals for larger PS particles (1 μm > 500 nm > 300 nm > 100 nm > 50 nm)[19] that is in good agreement with the data reported in the present study.

In terms of detecting other plastic types, a few studies have looked into detecting PET particles. Xu, G. *et al.* reported the detection of PET submicronplastics down to ~450 nm in size and PS submicronplastics down to ~360 nm in size on commercially available Klarite substrates.[38] Xu, D. *et al.* reported using AuSphere-doped filter paper to detect PET particles with sizes of 10–20 μm down to 0.1 g L^{-1} (100 ng mL^{-1}).[39] Yin *et al.* reported the preparation of PS, PET, PE, and PP microplastics with sizes between 80–150 μm to assess AuSphere-soaked sponge SERS substrates for their detection. However, they report a LOD only for PS microparticles (0.001 mg mL^{-1} or ~1 μg mL^{-1}).[40] It is thus clear that the 36 nm PET nanoplastics detected with the AuStars-based substrates presented in this study are currently the smallest PET detected with any SERS substrate reported to date. It can be difficult to draw direct conclusions from the further comparison of these studies due to such vast differences in particle size and substrate type, however, one trend appears to be the consistently higher efficiency of SERS substrates for the detection of PS particles over even other plastic types which contain aromatic rings like PET. Thus, the literature analyzed is in good agreement with the trend in results observed on AuStars substrates.

Finally, a few other studies have investigated the detection of PE or PP particles. Mikac *et al.* reported that through the use of AuSpheres or Au nanorods aggregated around plastic particles, they struggled to detect PE microplastics of 1–4 μm size even at concentrations of 200 μg mL^{-1}, but they could detect PS submicronplastics of 350 nm down to 6.5 μg mL^{-1}.[17] Additionally, Lv *et al.* employed a similar strategy with AgSpheres in an effort to detect 10 μm PE and PP microplastics.[15] At this size range, they reported it was possible to measure the signal for the PE and PP. However, the signal was only shown after adding an unspecified surfactant. They reported that the SERS enhancement of signal for microplastics was not as strong as those observed for PS nanoplastics (100 nm with LOD of 40 μg mL^{-1}).[15] Lv *et al.* further reported that the 500 nm PS submicronplastics they studied gave stronger signals than the 100 nm PS nanoplastics.[15] All of these findings further support what was observed with AuStars-based SERS substrates in this study. As such, it becomes clear that the properties of the plastic particles, namely their size and plastic type, directly influence the analytical capabilities of the SERS substrates prepared. It is particularly interesting to note that plastic types with aliphatic polymer backbones (*e.g.*, PE and PP) are difficult to detect even at the microplastic size range due to the low Raman cross-section.[31] Thus, studies that focus on further probing why such a drastic difference is observed and how this limitation could be surmounted would be particularly important in the future. A table summarizing all factors discussed here can be found in Table S3.†

Additional factors to consider

Within this study, the samples presented were measured only in a very simple matrix: Milli-Q water. Samples which are present in such a simple matrix can be studied extensively using SERS, and, if an optimized and shelf-stable SERS substrate can be obtained from an external source (*e.g.*, commercial providers or academic collaborators), the effort required to perform the analysis would be no more intensive than standard Raman spectroscopy. Thus, there is potential for employing SERS substrates such as the ones produced herein for research attempting to study changes in the chemical structure or physical properties of the particles being analyzed. As specific examples, it has already been demonstrated for larger sizes of plastics that Raman spectroscopy is viable for probing differences in crystallinity,[31,41] assessing presence of additives,[31,42] and determining sample degradation levels as a result of exposure to environmental conditions (*e.g.*, UV irradiation, mechanical forces from wind, waves, or other laboratory-based simulations of these phenomena) through detection of slight changes in the spectra.[31,43,44]

It is important to note, however, that for samples of plastic particles which are in more complex matrices there will likely be interference in the final spectra obtained. High amounts of additional organic or inorganic material in the sample matrix, or formation of protein or eco-coronas can place a layer of materials between the plastic particle of interest and the ~10 nm range from the SERS substrate surface where signal enhancement is known to occur.[14] Such sample behavior could strongly inhibit detection of the plastic signal; thus, the optimization of sample purification protocols may be of interest for future SERS works. Furthermore, truly quantitative SERS measurements are not a trivial matter, and would likely require the introduction of internal standards (*i.e.*, Raman reporter molecules at controlled concentrations) to normalize sample signal

against.[14] This would have to be considered for each individual plastic type of interest to ensure that the reporter molecule did not interfere with the plastic signal in the spectra acquired.

Finally, one could imagine an adaptation of the current analytical protocol which would facilitate SERS measurements at higher AuStars concentrations on the substrate surface. The most prominent example of how this could be achieved would be to increase the soaking time for substrate functionalization with AuStars, and then employ a different excitation laser line (*e.g.*, near 900 nm) to conduct the final measurements.[14] However, it is relevant to note that even without such system adaptations the AuStars-based SERS substrates produced herein detected nanoplastic particles (33 nm or 36 nm in size) at concentrations already within relevant ranges for laboratory-based toxicity studies.[45,46]

Conclusions

There is a great need in the field of submicron- and nanoplastics for the development of analytical protocols which can detect plastics without the need for sample destruction. This manuscript reports the successful optimization of a protocol for creating LbL assembled AuStars-based SERS substrates on glass slides. These substrates were employed to determine the LODs for 161 nm PS, 33 nm PS, 36 nm PET, 121 nm PP, and 126 nm PE particles. AuStars-based SERS substrates showed a marked improvement in LODs for 161 nm and 33 nm PS particles compared to their AuSpheres-based predecessors, with 161 nm PS detected at concentrations as low as 625 ng mL^{-1} and 33 nm PS down to 1.25 μg mL^{-1}. Furthermore, AuStars-based substrates were viable for detecting 36 nm PET, the smallest PET particles currently detected in SERS literature, at concentrations as low as 5 μg mL^{-1}. Despite their comparable size range, a difference in LOD was noted for 33 nm PS and 36 nm PET that hinted towards the potential influence of plastic type on SERS substrate performance. Despite their larger size, this observation was further highlighted by the inability to detect 126 nm PE and 121 nm PP particles.

Data availability

All raw data used to create the presented figures and tables is available on Zenodo under the following link: **https://doi.org/10.5281/zenodo.8143161**.

Author contributions

J. C. was responsible for plastic particle creation, some gold particle synthesis, substrate creation, acquisition and interpretation of data, and writing. P. T.-B. was the head co-investigator and was responsible for method creation and validation, some gold particle synthesis, and manuscript editing. L. R.-L. was responsible for manuscript editing and assisted with data interpretation. B. R.-R. was responsible for manuscript editing. A. P.-F. was responsible for manuscript editing and was the project's principal investigator. All authors have read and agreed to the published version of the manuscript.

Conflicts of interest

The authors declare no conflicts of interest.

Acknowledgements

J. C. and A. P.-F. acknowledge funding from the Swiss National Science Foundation (Grant no. 200020_184635). J. C., A. P.-F., and B. R.-R. thank the Adolphe Merkle Foundation for funding. Additionally, this work benefitted from support from the Swiss National Science Foundation through the National Center of Competence in Research Bio-Inspired Materials. P. T.-B. and L. R.-L. acknowledge funding from LAnd-Based Solutions for PLAStics in the Sea Project (LABPLAS, Grant Agreement no.: 101003954, financed by the EU H2020 program). L. R.-L. acknowledges funding from FCT (Fundação para a Ciência e Technologia) for the Scientific Employment Stimulus Program (2020.04021.CEECIND). The authors would like to thank Dr. Livius Muff, Dr. Roman Lehner, Prof. Christoph Weder, and Liliane Ackermann Hirschi for their support with particle synthesis.

References

1 J. Caldwell, P. Taladriz-Blanco, R. Lehner, A. Lubskyy, R. D. Ortuso and B. Rothen-Rutishauser, *et al.* The micro-, submicron-, and nanoplastic hunt: A review of detection methods for plastic particles, *Chemosphere*, 2022, **293**, 133514.

2 L. M. Hernandez, E. G. Xu, H. C. E. Larsson, R. Tahara, V. B. Maisuria and N. Tufenkji, Plastic Teabags Release Billions of Microparticles and Nanoparticles into Tea, *Environ. Sci. Technol.*, 2019, **53**(21), 12300–12310.

3 D. Materić, R. Holzinger and H. Niemann, Nanoplastics and ultrafine microplastic in the Dutch Wadden Sea – The hidden plastics debris?, *Sci. Total Environ.*, 2022, **846**, 157371.

4 A. Ter Halle, L. Jeanneau, M. Martignac, E. Jardé, B. Pedrono and L. Brach, *et al.* Nanoplastic in the North Atlantic Subtropical Gyre, *Environ. Sci. Technol.*, 2017, **51**(23), 13689–13697.

5 D. Materić, H. A. Kjær, P. Vallelonga, J.-L. Tison, T. Röckmann and R. Holzinger, Nanoplastics measurements in Northern and Southern polar ice, *Environ. Res.*, 2022, **208**, 112741.

6 Y. Xu, Q. Ou, X. Wang, F. Hou, P. Li and J. P. van der Hoek, *et al.* Assessing the Mass Concentration of Microplastics and Nanoplastics in Wastewater Treatment Plants by Pyrolysis Gas Chromatography–Mass Spectrometry, *Environ. Sci. Technol.*, 2023, **57**(8), 3114–3123.

7 L. Pang, Q. Lin, S. Zhao, H. Zheng, C. Li and J. Zhang, *et al.* Data quality assessment for studies investigating microplastics and nanoplastics in food products: Are current data reliable?, *Front. Environ. Sci. Eng.*, 2023, **17**(8), 94.

8 A. Masseroni, C. Rizzi, C. Urani and S. Villa, Nanoplastics: Status and Knowledge Gaps in the Finalization of Environmental Risk Assessments, *Toxics*, 2022, **10**(5), 270.
9 D. J. Gardiner, Introduction to Raman Scattering, in *Practical Raman Spectroscopy*, ed. D. J. Gardiner and P. R. Graves, Springer Berlin Heidelberg, Berlin, Heidelberg, 1989, pp. 1–12.
10 A. Käppler, D. Fischer, S. Oberbeckmann, G. Schernewski, M. Labrenz and K.-J. Eichhorn, *et al.* Analysis of environmental microplastics by vibrational microspectroscopy: FTIR, Raman or both?, *Anal. Bioanal. Chem.*, 2016, **408**(29), 8377–8391.
11 R. R. Jones, D. C. Hooper, L. Zhang, D. Wolverson and V. K. Valev, Raman Techniques: Fundamentals and Frontiers, *Nanoscale Res. Lett.*, 2019, **14**, 231.
12 L. Rayleigh, On the Theory of Optical Images, with special reference to the Microscope, *J. R. Microsc. Soc.*, 1903, **23**(4), 474–482.
13 R. Gillibert, G. Balakrishnan, Q. Deshoules, M. Tardivel, A. Magazzù and M. G. Donato, *et al.* Raman Tweezers for Small Microplastics and Nanoplastics Identification in Seawater, *Environ. Sci. Technol.*, 2019, **53**(15), 9003–9013.
14 J. Langer, D. J. de Aberasturi, J. Aizpurua, R. A. Alvarez-Puebla, B. Auguié and J. J. Baumberg, *et al.* Present and Future of Surface-Enhanced Raman Scattering, *ACS Nano*, 2020, **14**(1), 28–117.
15 L. Lv, L. He, S. Jiang, J. Chen, C. Zhou and J. Qu, *et al.* In situ surface-enhanced Raman spectroscopy for detecting microplastics and nanoplastics in aquatic environments, *Sci. Total Environ.*, 2020, **728**, 138449.
16 X.-X. Zhou, R. Liu, L.-T. Hao and J.-F. Liu, Identification of polystyrene nanoplastics using surface enhanced Raman spectroscopy, *Talanta*, 2021, **221**, 121552.
17 L. Mikac, I. Rigó, L. Himics, A. Tolić, M. Ivanda and M. Veres, Surface-enhanced Raman spectroscopy for the detection of microplastics, *Appl. Surf. Sci.*, 2023, **608**, 155239.
18 Y. Jeon, D. Kim, G. Kwon, K. Lee, C.-S. Oh and U.-J. Kim, *et al.* Detection of nanoplastics based on surface-enhanced Raman scattering with silver nanowire arrays on regenerated cellulose films, *Carbohydr. Polym.*, 2021, **272**, 118470.
19 Q. Yang, S. Zhang, J. Su, S. Li, X. Lv and J. Chen, *et al.* Identification of Trace Polystyrene Nanoplastics Down to 50 nm by the Hyphenated Method of Filtration and Surface-Enhanced Raman Spectroscopy Based on Silver Nanowire Membranes, *Environ. Sci. Technol.*, 2022, **56**(15), 10818–10828.
20 Y. Qin, J. Qiu, N. Tang, Y. Wu, W. Yao and Y. He, Controllable preparation of mesoporous spike gold nanocrystals for surface-enhanced Raman spectroscopy detection of micro/nanoplastics in water, *Environ. Res.*, 2023, **228**, 115926.
21 S. Kihara, A. Chan, E. In, N. Taleb, C. Tollemache and S. Yick, *et al.* Detecting polystyrene nanoplastics using filter paper-based surface-enhanced Raman spectroscopy, *RSC Adv.*, 2022, **12**(32), 20519–20522.
22 Q. T. Lê, N. H. Ly, M.-K. Kim, S. H. Lim, S. J. Son and K.-D. Zoh, *et al.* Nanostructured Raman substrates for the sensitive detection of submicrometer-sized plastic pollutants in water, *J. Hazard. Mater.*, 2021, **402**, 123499.
23 J. Caldwell, P. Taladriz-Blanco, B. Rothen-Rutishauser and A. Petri-Fink, Detection of Sub-Micro- and Nanoplastic Particles on Gold Nanoparticle-Based Substrates through Surface-Enhanced Raman Scattering (SERS) Spectroscopy, *Nanomaterials*, 2021, **11**(5), 1149.
24 B. Enustun and J. Turkevich, Coagulation of colloidal gold, *J. Am. Chem. Soc.*, 1963, **85**(21), 3317–3328.
25 K. R. Brown and M. J. Natan, Hydroxylamine Seeding of Colloidal Au Nanoparticles in Solution and on Surfaces, *Langmuir*, 1998, **14**(4), 726–728.
26 P. S. Kumar, I. Pastoriza-Santos, B. Rodríguez-González, F. J. G. de Abajo and L. M. Liz-Marzán, High-yield synthesis and optical response of gold nanostars, *Nanotechnology*, 2008, **19**, 015606.
27 L. F. Muff, S. Balog, J. Adamcik, C. Weder and R. Lehner, Preparation of Well-Defined Fluorescent Nanoplastic Particles by Confined Impinging Jet Mixing, *Environ. Sci. Technol.*, 2023, **57**(45), 17201–17211.
28 J. Stetefeld, S. A. McKenna and T. R. Patel, Dynamic light scattering: a practical guide and applications in biomedical sciences, *Biophys. Rev.*, 2016, **8**(4), 409–427.
29 B. Jasse, R. S. Chao and J. L. Koenig, Laser Raman scattering in uniaxially oriented atactic polystyrene, *J. Polym. Sci., Polym. Phys. Ed.*, 1978, **16**(12), 2157–2169.
30 E. Rebollar, S. Pérez, M. Hernández, C. Domingo, M. Martín and T. A. Ezquerra, *et al.* Physicochemical modifications accompanying UV laser induced surface structures on poly(ethylene terephthalate) and their effect on adhesion of mesenchymal cells, *Phys. Chem. Chem. Phys.*, 2014, **16**(33), 17551–17559.
31 V. Nava, M. L. Frezzotti and B. Leoni, Raman Spectroscopy for the Analysis of Microplastics in Aquatic Systems, *Appl. Spectrosc.*, 2021, **75**(11), 1341–1357.
32 E. Andreassen, *Infrared and Raman spectroscopy of polypropylene*, Springer, Dordrecht, Netherlands, 1999.
33 W. Xi and A. J. Haes, Elucidation of pH impacts on monosubstituted benzene derivatives using normal Raman and surface-enhanced Raman scattering, *J. Chem. Phys.*, 2020, **153**(18), 184707.
34 R. Aroca, *Surface-Enhanced Vibrational Spectroscopy*, Wiley, 2006.
35 D. Bhaumik, H. Jaffé and J. Mark, Calculated polarizabilities for some aliphatic and aromatic hydrocarbons, *J. Mol. Struct.: THEOCHEM*, 1982, **87**(1), 81–86.
36 F. G. Vogt and G. R. Williams, Analysis of a Nanocrystalline Polymer Dispersion of Ebselen Using Solid-State NMR, Raman Microscopy, and Powder X-ray Diffraction, *Pharm. Res.*, 2012, **29**(7), 1866–1881.
37 P. Bock and N. Gierlinger, Infrared and Raman spectra of lignin substructures: Coniferyl alcohol, abietin, and coniferyl aldehyde, *J. Raman Spectrosc.*, 2019, **50**(6), 778–792.
38 G. Xu, H. Cheng, R. Jones, Y. Feng, K. Gong and K. Li, *et al.* Surface-Enhanced Raman Spectroscopy Facilitates the Detection of Microplastics <1 μm in the Environment, *Environ. Sci. Technol.*, 2020, **54**(24), 15594–15603.
39 D. Xu, W. Su, H. Lu, Y. Luo, T. Yi and J. Wu, *et al.* A gold nanoparticle doped flexible substrate for microplastics

SERS detection, *Phys. Chem. Chem. Phys.*, 2022, **24**(19), 12036–12042.

40 R. Yin, H. Ge, H. Chen, J. Du, Z. Sun and H. Tan, *et al.* Sensitive and rapid detection of trace microplastics concentrated through Au-nanoparticle-decorated sponge on the basis of surface-enhanced Raman spectroscopy, *Environ. Adv.*, 2021, **5**, 100096.

41 A. S. Nielsen, D. N. Batchelder and R. Pyrz, Estimation of crystallinity of isotactic polypropylene using Raman spectroscopy, *Polymer*, 2002, **43**(9), 2671–2676.

42 B. E. Oßmann, G. Sarau, H. Holtmannspötter, M. Pischetsrieder, S. H. Christiansen and W. Dicke, Small-sized microplastics and pigmented particles in bottled mineral water, *Water Res.*, 2018, **141**, 307–316.

43 L. Cai, J. Wang, J. Peng, Z. Wu and X. Tan, Observation of the degradation of three types of plastic pellets exposed to UV irradiation in three different environments, *Sci. Total Environ.*, 2018, **628–629**, 740–747.

44 M. Dong, Q. Zhang, X. Xing, W. Chen, Z. She and Z. Luo, Raman spectra and surface changes of microplastics weathered under natural environments, *Sci. Total Environ.*, 2020, **739**, 139990.

45 R. Qiao, M. Mortimer, J. Richter, B. Rani-Borges, Z. Yu and M. Heinlaan, *et al.* Hazard of polystyrene micro-and nanospheres to selected aquatic and terrestrial organisms, *Sci. Total Environ.*, 2022, **853**, 158560.

46 J.-L. Xu, X. Lin, J. J. Wang and A. A. Gowen, A review of potential human health impacts of micro- and nanoplastics exposure, *Sci. Total Environ.*, 2022, **851**, 158111.